ACS APPLIED MATERIALS & INTERFACES

Research Article

www.acsami.org

All-Solid-State High-Energy Asymmetric Supercapacitors Enabled by Three-Dimensional Mixed-Valent MnO_x Nanospike and Graphene Electrodes

Jie Yang,[†,‡] Guizhu Li,[†,§] Zhenghui Pan,[†] Meinan Liu,[†] Yuan Hou,[†] Yijun Xu,[†] Hong Deng,[§] Leimei Sheng,[‡] Xinluo Zhao,[*,‡] Yongcai Qiu,[*,#,⊥] and Yuegang Zhang[*,†,⊥]

[†]*i*-Lab, Suzhou Institute of Nano-Tech and Nano-Bionics, Chinese Academy of Science, Suzhou 215123, China

[‡]Department of Physics, Institute of Low-Dimensional Carbons and Device Physics, Shanghai University, Shanghai 200444, China,

[§]School of Chemistry and Environment, South China Normal University, Guangzhou 510006, China

[#]Department of Materials Science and Engineering, Stanford University, Stanford, California 94305, United States

[⊥]Department of Physics, Tsinghua University, Beijing 100084, China

Supporting Information

ABSTRACT: Three-dimensional (3D) nanostructures enable high-energy storage devices. Here we report a 3D manganese oxide nanospike (NSP) array electrode fabricated by anodization and subsequent electrodeposition. All-solid-state asymmetric supercapacitors were assembled with the 3D Al@Ni@MnO_x NSP as the positive electrode, chemically converted graphene (CCG) as the negative electrode, and Na_2SO_4/poly(vinyl alcohol) (PVA) as the polymer gel electrolyte. Taking advantage of the different potential windows of Al@Ni@MnO_x NSP and CCG electrodes, the asymmetric supercapacitor showed an ideal capacitive behavior with a cell voltage up to 1.8 V, capable of lighting up a red LED indicator (nominal voltage of 1.8 V). The device could deliver an energy density of 23.02 W h kg^{-1} at a current density of 1 A g^{-1}. It could also preserve 96.3% of its initial capacitance at a current density of 2 A g^{-1} after 10000 charging/discharging cycles. The remarkable performance is attributed to the unique 3D NSP array structure that could play an important role in increasing the effective electrode surface area, facilitating electrolyte permeation, and shortening the electron pathway in the active materials.

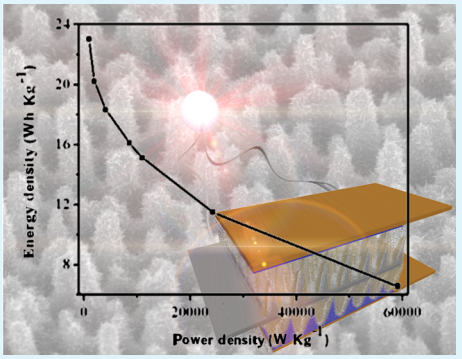

KEYWORDS: *all-solid-state, asymmetric supercapacitors, three-dimensional, MnO_x nanospike, chemically converted graphene*

INTRODUCTION

As the global energy shortage and environmental pollution problems become increasingly serious, it is urgently necessary to develop high-performance energy storage devices.[1−4] Supercapacitors have been one of the most promising candidates in the field of energy storage due to their high power density, fast charge/discharge rate, and long-cycle lifetime.[5−9] However, to meet the requirement of practical applications, further improvement of energy density and operating voltage of supercapacitors is needed.[10,11] According to the equation $E = 1/2CV^2$, a capacitor's storage energy E can be enhanced by increasing its capacitance C or, more significantly, by increasing the operating voltage V.[12]

An effective approach to increase capacitance C is to use pseudocapacitive materials such as MnO_x, NiO, CoO_x, RuO_2, $Co(OH)_2$, and $Ni(OH)_2$, which show much higher capacitive performance.[13−15] Among them, MnO_x was widely studied owing to its low cost, eco-friendliness, natural abundance, and high theoretical capacitance (>1300 F g^{-1}).[16] However, the practical application of MnO_x-based supercapacitors was limited by the low electric conductivity of the active material.[17,18] One of the solutions to resolve this problem is to coat nanostructured MnO_x on a 3D conductive network. Well-designed 3D electrodes such as 3D reduced graphene oxide (rGO)-CNT,[19] 3D $ZnCo_2O_4$ nanocone forests,[20] and 3D Au nanocone[21] can shorten the electron transfer pathway and increase the contact area between electrolytes and active materials. However, the current approach has problems such as low energy density, complex fabrication process, high cost, and relatively poor cycling stability. On the basis of the above considerations, we designed and fabricated a 3D Al@Ni@MnO_x nanospike (NSP) array as a positive electrode. The electrode was obtained by combining simple anodization and electrodeposition methods without using complex processes such as nano-imprinting. The unique nanostructure of the 3D Al@Ni@MnO_x NSP structure could improve electron transfer kinetics, shorten the electron transfer pathway, and increase the contact area between electrolytes and active materials.

Received: May 9, 2015
Accepted: September 22, 2015
Published: September 22, 2015

DOI: 10.1021/acsami.5b07849
ACS Appl. Mater. Interfaces 2015, 7, 22172−22180

Table 1. Comparisons of the MnO_x-Based Asymmetric Supercapacitors

electrode materials		electrochemical characteristics						
positive	negative	U_{max} (V)	E (Wh kg^{-1})	P (W kg^{-1})	E (mW h cm^{-3})	P (W cm^{-3})	electrolyte	cycle no.
MnO_2[34]	Fe_3O_4	1.8	8.1	10200			K_2SO_4	5000
MnO_2[49]	AC	2	21.0	123			KNO_3	1000, 88%
MnO_2[24]	FeOOH	1.85	12	3700			Li_2SO_4	2000, 85%
MnO_2@CNT@textile[33]	reduced MnO_2@CNT@ textile	1	5−20	13000			Na_2SO_4	50000, 80%
graphene@MnO_2[48]	graphene	1.7	10.03	2530			Na_2SO_4	10000, 69%
GHCS@MnO_2[45]	GHCS	2.0	22.1	7000			Na_2SO_4	1000, 97.3%
H-TiO_2@MnO_2 core−shell NWs[53]	H-TiO_2@C core−shell NWs				0.30	0.23	LiCl/PVA	5000, 91.2%
rGO[52]	MnO_{2-x} NRs nanorods				0.25	1.44	LiCl/PVA	
MnO_2@rGO hydrogel[22]	rGO hydrogel	1.6	21.2	820			Na_2SO_4	1000, 89.6%
MnO_2@ZnO[36]	HI-rGO	1.8			0.234	0.133	LiCl/PVA	5000, 98.5%
$Ni(OH)_2$@NGP[51]	Mn_3O_4@NGP	1.3			0.35	0.0325	PVA/NaOH	12000, 82.1%
MnO_2@$MnCO_3$@rGO[46]	rGO	1.6	17.8	400			Na_2SO_4	2000, 84.1%
MnO_2@C spheres[47]	AC	2.0	19.9	500			$LiNO_3$	1000, 96.6%
CF@RGO@MnO_2[50]	CF@TRGO	1.6			1.23	0.27	PAAK/KCl	10000, 91%
a-MnO_x@rGO @$CNT_{1.25\ V}$[19]	AC	2.0	18	1000			Na_2SO_4	
3D Al@Ni@MnO_x NSP	CCG	1.8	23.02	947.11	1.29	0.053	PVA/Na_2SO_4	10000, 96.3%

Another way to enhance energy density is to broaden the operation voltage. Recently, intensive efforts have been devoted to fabricating MnO_x-based asymmetric supercapacitors, and a variety of negative electrode materials have been developed. For instance, Wu et al. designed asymmetric supercapacitors by using MnO_2/rGO hydrogel as the positive electrode and a pure rGO hydrogel as the negative electrode.[22] Besides, MnO_2@graphene//carbon nanofibers,[23] MnO_2//FeOOH,[24] and MnO_2//PPy (polypyrrole)[25] were also applied to assemble asymmetric supercapacitors. Among all of the negative materials, carbonaceous materials with high specific surface area and moderate cost are the most widely used. In this paper, we used a chemically converted graphene (CCG) as the negative electrode, considering its high capacitance of >200 F g^{-1}, high conductivity, chemical stability, and large surface area.[30]

From safety and portability considerations, asymmetric supercapacitors using solid-state electrolytes are highly desirable for future consumer electronics.[26] Replacement of the liquid electrolyte by a solid one could not only increase the operating temperature of supercapacitors but also enhance the mechanical strength, reduce the weight, and enhance the chemical stability and flexibility.[4,27−29] For example, Wu et al. successfully developed Ni@GF@MnO_2//Ni@GF@PPy (PVA/KOH),[54] Qiu et al. fabricated MnO_x@Au nanocone//CCG (PVA/Na_2SO_4),[21] and Lu et al. developed H-TiO_2@MnO_2//H-TiO_2@C (PVA/LiCl).[53] Most of these systems achieved high energy densities; however, their relatively poor cycling stability remains a great challenge for practical applications.

In this work, we have successfully developed an all-solid-state MnO_x-based asymmetric supercapacitors enabled by 3D Al@Ni@MnO_x NSP structure as the positive electrode and CCG as the negative electrode. After assembly with a solid Na_2SO_4/PVA electrolyte, we obtained an all-solid-state supercapacitor with a potential of 1.8 V that could deliver a higher energy density of 23.02 W h kg^{-1} at a current density of 1 A g^{-1}, much higher than those of other MnO_x-based supercapacitors reported previously.[31−34] Our device also preserves 96.3% of its initial capacitance at a current density of 2 A g^{-1} after 10000 charging/discharging cycles. In comparison with those from the literature (Table 1), such a rationally designed supercapacitor shows advantages in energy density and cycling stability. This facilely fabricated, low cost, environmentally friendly, and safe all-solid-state asymmetric supercapacitor has great potential in future commercial applications.

EXPERIMENTAL SECTION

Chemicals. Aluminum (Al) foil (99%, with 0.1 mm thickness), citric acid ($C_6H_8O_7·H_2O$, 99%, Sinopharm Chemical Reagent Co. Ltd.), ethylene glycol ($C_2H_4O_2$, 99%, Sinopharm Chemical Reagent Co. Ltd.), graphite (C, powder, <150 μm, Sigma-Aldrich), hydrazine hydrate solution ($N_2H_4·H_2O$, 24−26% in water, Sigma-Aldrich), ammonia solution ($NH_3·H_2O$, 28 wt % in water, Aladdin), manganese sulfate ($MnSO_4$, 99%, Sinopharm Chemical Reagent Co. Ltd.), sodium acetate ($C_2H_3NaO_2$, 99%, Sinopharm Chemical Reagent Co. Ltd.), poly(vinyl alcohol) (PVA, $[CH_2CH(OH)]_n$, n = 1799, Aladdin), and sodium sulfate (Na_2SO_4, 98%, Sinopharm Chemical Reagent Co. Ltd.) were used directly without any further purification.

3D Al NSP Array Electrode Preparation. Sheets of aluminum foil with a thickness of 0.1 mm were cut into 1.5 cm by 3 cm pieces. The acetone and isopropyl alcohol cleaned Al foil was used as the working electrode, and a carbon rod was used as the counter electrode in a homemade anodization setup. Anodization was carried out under a 400 V DC voltage in a mixed solution of 4 wt % citric acid and ethylene glycol (v/v = 1:1). An anodic alumina membrane (AAM) of a few micrometer thickness on the Al substrate could be formed after anodization for 13 h at 28 °C. Then, the alumina was etched away in a mixture of phosphoric acid (6 wt %) and chromic acid (1.8 wt %) at 63 °C for 60 min to form an Al NSP array. The as-obtained Al NSP chips were cleaned with deionized water and enthanol and then dried at room temperature for the subsequent Ni thin film deposition.

Preparation of 3D Al@Ni@MnO_x NSP Array Electrode and MnO_x Flat Electrode. A conductive Ni thin film of 100−150 nm thickness was sputtered on Al NSP array electrodes by magnetron sputtering. MnO_x coating was performed using a facile one-step electrodeposition method in an aqueous solution of 0.5 M $MnSO_4$ and 0.5 M CH_3COONa with a current density of 0.5 mA cm^{-2}, using a saturated calomel electrode (SCE) (type 232, saturated solution) as the reference and platinum (Pt) (Pt 310, 10 mm × 10 mm) as the counter electrode. A MnO_x flat electrode was prepared in the same way on the flat Al/Ni substrate. To avoid the electrolyte residual or align species existing on the surface of the deposited layers, we

DOI: 10.1021/acsami.5b07849
ACS Appl. Mater. Interfaces 2015, 7, 22172−22180

carefully rinsed the surface with deionized water several times and then dried it with air for the subsequent electrochemical test.

Preparation of CCG Electrode. CCG was prepared according to our previous study.[30] Briefly, 0.05 wt % graphene oxide solution was synthesized according to a modified Hummers method, and the obtained solution (30 mL) was mixed with 210 μL of hydrazine solution (35 wt % in water) and 210 μL of ammonia solution (28 wt % in water) in a 50 mL glass vial. After being vigorously shaken or stirred for a few minutes, the vial was sealed in a steel autoclave and kept in an electrical oven at 100 °C for 3 h. After the steel autoclave was naturally cooled to room temperature, 30 mL of the as-obtained CCG dispersion was vacuum filtered through a mixed cellulose ester filter membrane (0.05 μm pore size). The vacuum pump was stopped immediately once no free CCG dispersion was left on the filter cake. The CCG hydrogel films were then carefully peeled from the filter membrane, immediately transferred to a Petri dish, and immersed in water overnight to further remove the remaining ammonia and hydrazine. The microscopic characterizations of the CCG are shown in Figure S1.

Assembly of All-Solid-State Asymmetric Supercapacitors. The gel electrolyte was fabricated by mixing 6 g of Na_2SO_4 and 6 g of PVA in 60 mL of deionized water under vigorous stirring at 80 °C for 1 h. The 3D Al@Ni@MnO_x NSP array electrode and the CCG electrode were immersed in the clear solution of Na_2SO_4/PVA gel electrolyte for 60 min. The resulting electrolyte-filled electrodes were solidified for 12 h at room temperature. Finally, the devices were assembled with the as-prepared electrodes in the following order: PET/Au foil−CCG elecdtrode−solid electrolyte−Al@Ni@MnO_x NSP array electrode−solid electrolyte−CCG electrode−PET/Au foil. The terminals were clipped by toothless alligator clips, which were then connected to a CHI 660C electrochemical workstation for electrochemical characterization.

Characterization. The microstructure of the samples was characterized using a Quanta 400 FEG field-emission scanning electron microscope (FE-SEM) and a Tecnai G2 F20 S-Twin field-emission transmission electron microscope (FE-TEM). The electrochemical properties of the samples were measured by a CHI 660C electrochemical workstation (CH Instruments Inc.); XPS characterization was performed on an Axis Ultra DLD X-ray photoelectron spectroscope.

RESULTS AND DISCUSSION

Schematic Diagram of the Fabrication Process. The fabrication process of the all-solid-state asymmetric supercapacitor involved four main steps, as shown in Figure 1. First, a random 3D Al nanospike (NSP) array was fabricated on both sides of thin Al foil. The details of the anodization and etching processes can be found under Experimental Section. Second, a thin layer of a highly conductive Ni metal with a thickness of 100 nm was coated on the 3D Al NSPs by magnetron sputtering. The Ni coating improves water wettability of the 3D Al NSPs and prevents Al from etching by electrolyte during the subsequent electrodeposition. It also enhances the mechanical strength of 3D Al NSP current collector. Third, an active MnO_x layer was coated on the 3D Al@Ni NSP array by electrodeposition in an aqueous solution of 0.5 M $MnSO_4$ and 0.5 M CH_3COONa with a current density of 0.5 mA cm^{-2}. Finally, the all-solid-state supercapacitors were assembled following the steps described under Experimental Section.

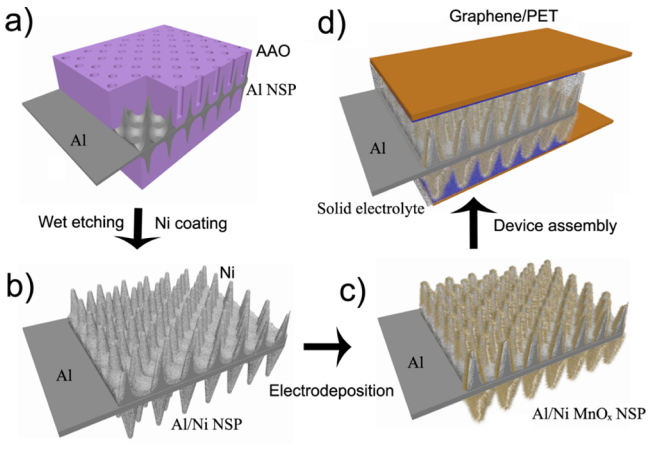

Figure 1. Schematic diagram of the fabrication process of the 3D Al@Ni NSP electrode and the all-solid-state asymmetric supercapacitor: (a) anodization and etching Al foil; (b) magnetron sputtering Ni on Al nanospikes; (c) electrodeposition MnO_x on 3D Al@Ni NSP electrode; (d) assemble the device.

The morphology of the 3D Al NSP array was characterized by scanning electron microscopy (SEM). Figure 2a shows its 45° tilted-angle-view SEM image. It can be clearly seen that the dimple size of the anodized Al array is ~1 μm due to the self-organizing effect during AAM pore growth.[35] The heights of NSPs grown on the Al substrate are between 1 and 2.5 μm. Figure 2b shows the typical SEM images of the as-prepared 3D Al@Ni@MnO_x NSP electrode. Each nanospike is homogeneously covered with numerous ultrathin MnO_x nanosheets, which can clearly be seen from the transmission electron microscope (TEM) images (Figure 2c). The thickness of the MnO_x nanosheets layer can be adjusted (from about 20 to 120 nm) by changing the deposition time. Longer deposition time results in a thicker MnO_x layer (Figure S2). The morphologies of 3D Al@Ni@MnO_x NSP electrodes with various deposition time are shown in Figure S3. For comparison, MnO_x nanosheets electrodeposited on planar Ni/Al electrodes were also prepared. The MnO_x nanosheets appear to be randomly grown on the planar Ni/Al electrodes (Figure 2d).

Electrochemical Characterizations of the 3D Al@Ni@MnO_x NSP Electrode and MnO_x Flat Electrode. To evaluate the electrochemical behaviors of the 3D Al@Ni@MnO_x NSP electrode and the MnO_x flat electrode, we performed electrochemical measurements using 1 M Na_2SO_4 electrolyte in a three-electrode cell with a voltage window between 0 and 0.8 V. The details for electrochemical testing and characterization in the three-electrode cell are shown in the Supporting Information. The electrochemical impedance spectroscopy (EIS) measurement was conducted in the frequency range from 100 mHz to 200 kHz. As shown in Figure 3a, the 3D Al@Ni@MnO_x NSP electrode exhibited a typical capacitive behavior as the EIS curve was a nearly vertical line in the low-frequency region. The charge-transfer resistance of the 3D Al@Ni@MnO_x NSP electrode was much smaller than that of the flat one, as indicated by the smaller diameter of the semicircle in the impedance spectrum (inset of Figure 3a). These results indicated that the conductivity of the 3D electrode is much better than that of the flat one. To further investigate the advantage of the 3D Al@Ni@MnO_x NSP electrode, we compared cyclic voltammetry (CV) curves of the Al@Ni@MnO_x NSP (with Ni), flat MnO_x (with Ni), and pure Ni NSP electrodes at a scan rate of 50 mV s^{-1} (Figure 3b). The integrated CV area of the 3D Al@Ni@MnO_x NSP electrode is apparently larger than that of the flat samples. The redox peaks were clearly observed in the CV curves of the 3D Al@Ni@MnO_x NSP electrode (oxidation peak. 0.58 V; reduction peak. 0.47 V) and MnO_x flat electrode (oxidation peak, 0.63 V; reduction peak, 0.34 V), but were absent in the CV curve of pure Ni NSP electrode (Figure 3b; Figure S4), indicating that

DOI: 10.1021/acsami.5b07849
ACS Appl. Mater. Interfaces 2015, 7, 22172−22180

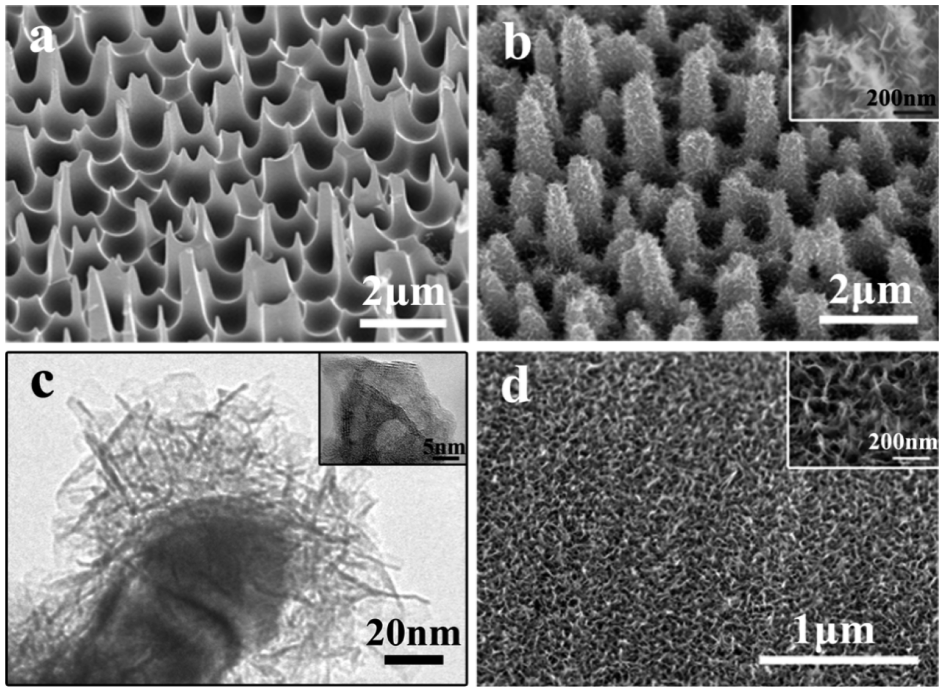

Figure 2. (a) SEM image of Al NSP array electrode obtained through anodization and etching processes; (b) SEM images of the electrodeposited MnO_x on the Ni-coated Al NSP array electrode (the inset shows its corresponding zoom-in view); (c) TEM images of the electrodeposited MnO_x on the Ni-coated Al NSP array electrode with a deposition time of 10 min (the inset shows its corresponding zoom-in view); (d) SEM images of the electrodeposited MnO_x on planar Ni electrode (the inset shows its corresponding zoom-in view).

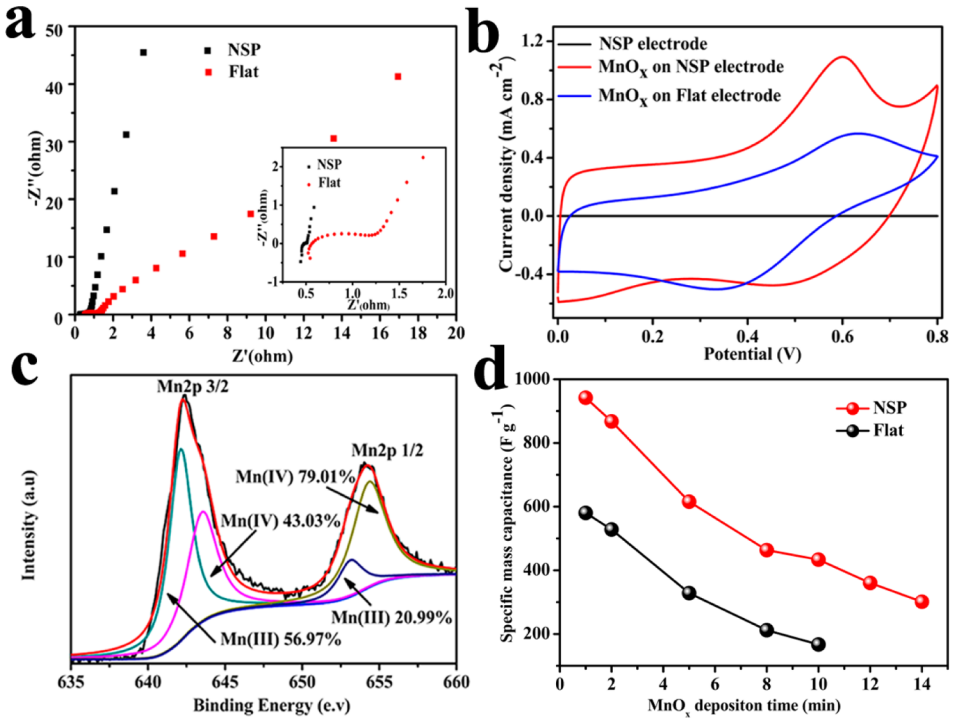

Figure 3. (a) Electrochemical impedance spectra of MnO_x on 3D Al@Ni NSP and flat substrates; (b) comparisons of CV curves of the 3D Al@Ni MnO_x NSP (with Ni), flat MnO_x (with Ni), and pure Ni NSP electrodes, respectively, at a scan rate of 50 mV s^{-1} (the MnO_x samples were prepared with a electrodeposition time of 1 min); (c) high-resolution XPS spectra of the Mn 2p taken on the 3D MnO_x NSP electrode; (d) specific mass capacitances of the 3D Al@Ni MnO_x NSP electrodes and flat MnO_x electrodes as a function of different MnO_x deposition time, measured with a scan rate of 50 mV s^{-1} in 1 M Na_2SO_4.

the capacitance comes from the combination of both electrochemical double-layer capacitance and pseudocapacitance generated by faradic redox reactions of mixed-valence MnO_x. The redox peaks can be assigned to the reaction Mn (III) ⇔ Mn(II) + e^-. The mixed-valence Mn ions were confirmed by the high-resolution XPS spectra of Mn 2p, as

DOI: 10.1021/acsami.5b07849
ACS Appl. Mater. Interfaces 2015, 7, 22172−22180

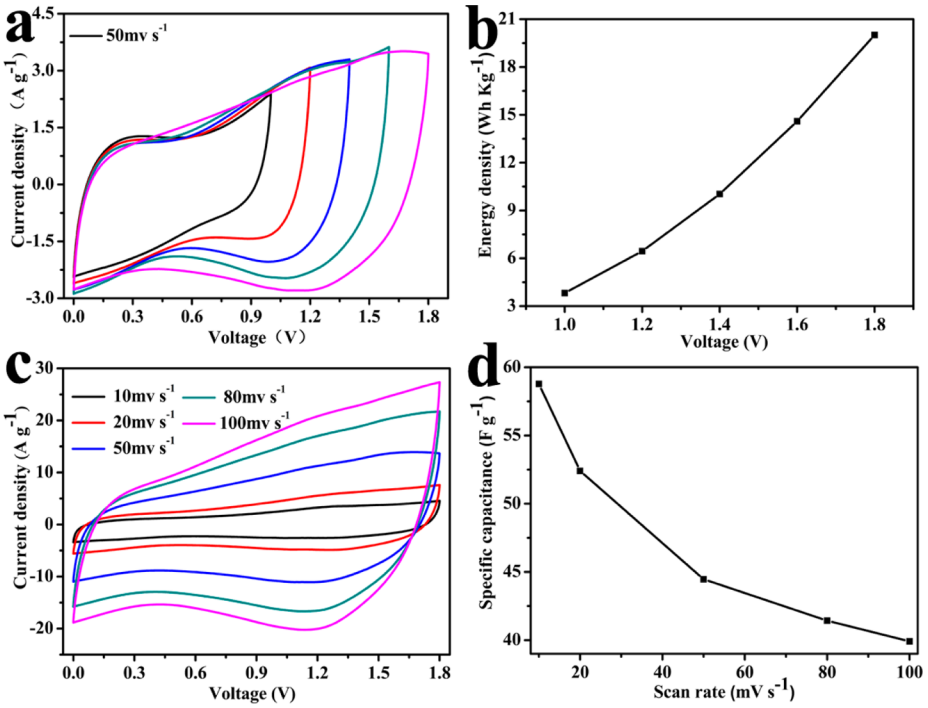

Figure 4. Electrochemical characterizations of the all-solid-state 3D Al@Ni@MnO_x//CCG asymmetric supercapacitor: (a) CV curves of the asymmetric supercapacitor at various potentials between 1.0 and 1.8 V in a Na_2SO_4/PVA electrolyte; (b) corresponding energy density as a function of voltage window; (c) CV curves of the asymmetric supercapacitor measured in the potential window from 0 to 1.8 V under different scan rates; (d) corresponding specific capacitances as a function of different scan rates.

shown in Figure 3c. The two major XPS peaks (642.3 and 654.2 eV) correspond to the spin orbit doublet of Mn $2p_{3/2}$ and Mn $2p_{1/2}$, respectively.[36] Each of the Mn $2p_{3/2}$ and Mn $2p_{1/2}$ peaks can be divided into two subpeaks of Mn $2p_{3/2}$ at 642.1 and 643.5 eV and Mn $2p_{1/2}$ at 653.2 and 654.4 eV, which can be assigned to Mn^{3+} and Mn^{4+} species in MnO_x.[37] The amount of each oxide phase can be estimated to be Mn^{3+} 21.0% and Mn^{4+} 79.0%. Thus, MnO_2 exists as the major manganese oxide phase in our 3D Al@Ni@MnO_x NSP electrode. The existence of other Mn oxidation states in the MnO_x phase, such as Mn_3O_4 and MnOOH,[38−40] can enhance rates of the surface redox reaction.[41] Given the same active material loading, the 3D Al@Ni@MnO_x NSP electrode has a much thinner active material layer than that of the flat MnO_x electrode due to the large difference of their effective surface areas. It has been proved that the thickness of MnO_x nanosheets has an effect on the electrochemical performance, and the thinner sheets with more active reaction sites would enhance the faradic surface charge storage.[6] On the other hand, the same effective surface area and higher active material loading results in higher total capacitance, but lower specific capacitance (Figure 3d). The different thicknesses of MnO_x nanosheets (obtained at different deposition times) also led to different overpotentials and thus different redox peak positions for both NSP electrode and flat electrode (Figure S5). Whereas all of the Mn surface atoms are involved in the pseudocapacitive process, charge transfer during charging/discharging also involved bulk insertion/extraction of cations into/from the MnO_x electroactive material.[42] With the increase of electrodeposition time, more and more MnO_x active material is deposited on the 3D NSP electrode and flat electrode, resulting in a higher specific volumetric capacitance (Figure S6). The volumetric capacitance of the 3D Al@Ni@MnO_x NSP electrodes reached the highest value of 4.22 F cm^{-3} with 10 min of MnO_x deposition. The highest specific mass capacitance of 942.2 F g^{-1} was obtained with a deposition time of 1 min, nearly 1.62 times higher than that of the MnO_x deposited on the flat substrate. The gradual decrease of mass capacitance is a result of the poor intrinsic conductivity of MnO_x and electrolyte diffusion limitation in a restricted space.[6] Compared with the flat electrode, the 3D Al@Ni@MnO_x NSP electrode exhibits a much better performance in both volumetric capacitance and specific mass capacitance under identical electrodeposition conditions (Figure S6).

Electrochemical Characterizations of the All-Solid-State Al@Ni@MnO_x//CCG Asymmetric Supercapacitor. Asymmetric all-solid-state supercapacitors were assembled as described under Experimental Section, and the details for electrochemical testing and characterization methods are shown in the Supporting Information. The results of CV measurements of the supercapacitors are shown in Figure 4a. Taking advantage of the different stable potential windows of 3D Al@Ni@MnO_x NSP and CCG electrodes (stable potential window = 0.8−0.0 V for the 3D Al@Ni@MnO_x NSP, 0.0 to −1.0 V for the CCG[22]), the asymmetric supercapacitor showed an ideal capacitive behavior with a cell voltage up to 1.8 V at a scan rate of 50 mV s^{-1}. As the energy density is proportional to the square of the voltage, the enlarged potential window gives rise to a remarkably enhanced energy density of the supercapacitors.[43] As shown in Figure 4b, the energy density significantly increases from 3.82 to 20.01 W h kg^{-1} with the operation voltage increasing from 1.0 to 1.8 V, suggesting that the stored energy can be improved at least by 424%.[23] Operation at a higher voltage also means that one can reduce the number of supercapacitors in series to achieve the desired output voltage.[6] In Figure 4c, the electrochemical performance of our asymmetric supercapacitors was evaluated by CV tests in

DOI: 10.1021/acsami.5b07849
ACS Appl. Mater. Interfaces 2015, 7, 22172−22180

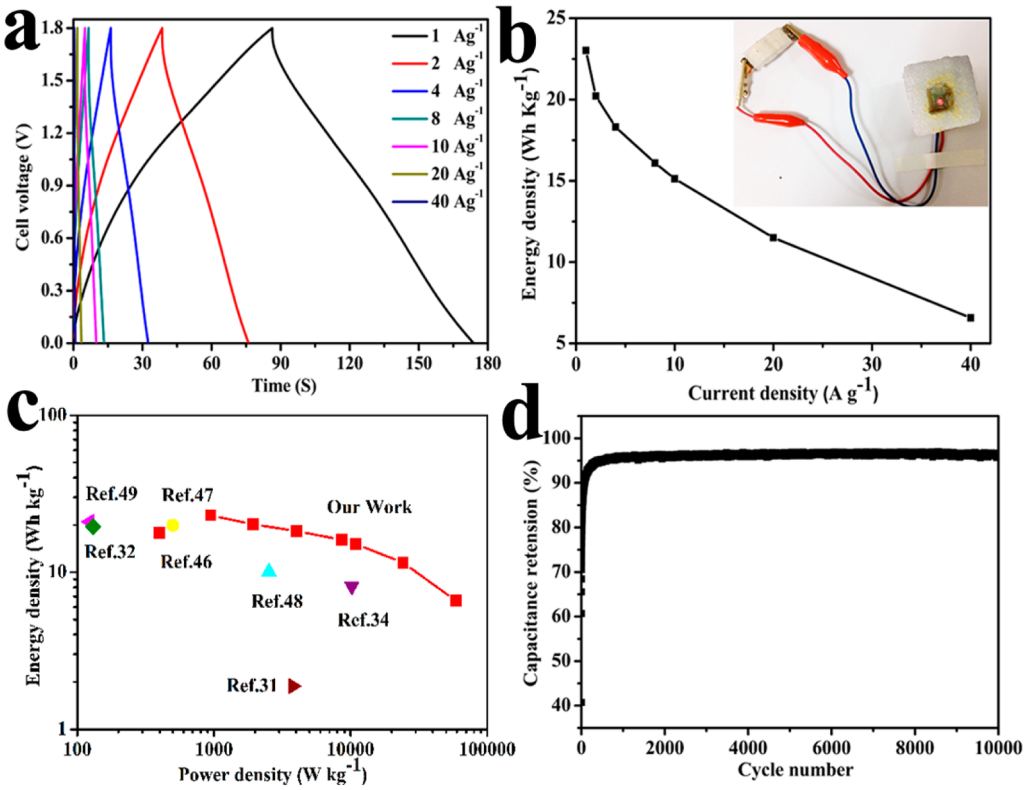

Figure 5. Galvanostatic charge/discharge measurements of the asymmetric supercapacitor consisting of the 3D Al@Ni@MnO_x NSP positive electrode and CCG negative electrode: (a) charge/discharge curves at various current densities; (b) corresponding energy densities as a function of current densities (the inset shows an optical image of the asymmetric supercapacitor (3D Al@Ni@MnO_x//CCG) lighting up a red LED indicator); (c) energy densities as a function of power densities; (d) cycling stability over 10000 cycles of the asymmetric supercapacitor.

the voltage window from 0 to 1.8 V at different scan rates from 10 to 100 mV s^{-1}. These CV curves remained a roughly rectangular shape with increasing scan rate, even at a high scan rate of 100 mV s^{-1}, which demonstrated the remarkably fast charge/discharge properties and high power density of the asymmetric supercapacitor.[44] The calculated specific capacitances were 58.78, 52.41, 44.47, 41.43, 39.91, and 8.39 F g^{-1}, respectively, in proper sequence according to scan rates of 10, 20, 50, 80, and 100 mV s^{-1} (Figure 4d). The gradual decrease of specific capacitance can be explained by the fact that the diffusion of the electrolytic ions deeper into the valleys was hindered at higher scan rates and only the outer surface of the active material was used for charge storage.[6]

Galvanostatic charge/discharge of an asymmetric supercapacitor was performed in various current densities with the voltage range of 0−1.8 V (Figure 5a). It can be seen that all of the charging curves were almost symmetric to their corresponding discharge counterparts and behaved as good linear voltage−time profiles. These results indicated our 3D micro/nano-interconnected structure had a rapid I−V response, a small equivalent series resistance, and an ideal capacitive characteristic, which were also confirmed by CV curves (Figure 4c).[23] Our 3D Al@Ni@MnO_x NSP//CCG asymmetric supercapacitor had a very small internal resistance (IR drop (V) = 0.00145 + 0.01471x, where x indicated the current density (A g^{-1})), which is beneficial for high discharge power delivery in practical applications (Figure S7). In Figure 5b, the energy density of the asymmetric capacitance was calculated to be 23.02 W h kg^{-1} on the basis of the total mass of active materials in both electrodes at a current density of 1 A g^{-1}. It still reached 6.57 W h kg^{-1} even at a high current density of 40 A g^{-1}. This excellent rate performance is comparable to or higher than those previously reported for MnO_x-based asymmetric supercapacitors MnO_x@rGO−$CNT_{1.25\ V}$//AC (18 W h kg^{-1}),[19] MnO_2@rGO hydrogel//rGO hydrogel (21.2 W h kg^{-1}),[22] GHCS@MnO_2//GHCS (22.1 W h kg^{-1}),[45] and MnO_2//FeOOH (12 W h kg^{-1}).[24] This all-solid-state 3D Al@Ni@MnO_x NSP//CCG asymmetric supercapacitor when fully charged can light up a red LED indicator of a nominal voltage of 1.8 V (inset of Figure 5b). To further demonstrate the supercapacitors' electrochemical performance, their energy and power densities were calculated and are shown in the Ragone plot of Figure 5c. It can be seen that the 3D Al@Ni@MnO_x NSP//CCG supercapacitor could deliver a high energy density without sacrificing power density. For example, when the power density reached to 59130 W kg^{-1}, the supercapacitor could still deliver 6.57 W h kg^{-1}. It is worth noting that the maximum energy obtained was 23.02 W h kg^{-1} under a power density of 947.11 W kg^{-1} (at a current density of 1 A g^{-1}). The energy density in this work is higher than or comparable to those of many previously reported devices (Table 1), such as MnO_2@$MnCO_3$@rGO aerogel//rGO aerogel (17.8 W h kg^{-1}, 400 W kg^{-1}),[46] MnO_2@C spheres//AC (19.9 W h kg^{-1}, 500 W kg^{-1}),[47] graphene@MnO_2//graphene (10.03 W h kg^{-1}, 2530 W kg^{-1}),[48] MnO_2//Fe_3O_4 (8.1 W h kg^{-1}, 10200 W kg^{-1}),[34] and MnO_2//AC (21.0 W h kg^{-1}, 123 W kg^{-1}),[49] as well as the target of the Partnership for a New Generation of Vehicles (15 W h kg^{-1}), indicating the feasibility for application in hybrid vehicle systems.

To further investigate the capacitive behaviors of our devices, their areal capacitance and volumetric capacitance were also calculated. The volumetric of the device was about 0.0109 cm^3

DOI: 10.1021/acsami.5b07849
ACS Appl. Mater. Interfaces 2015, 7, 22172−22180

(Figure S8). The areal capacitance and volumetric capacitance for the device were evaluated to be about 28.6 mF cm^{-2} and 2.83 F cm^{-3}, respectively, at a current density of 0.6 mA cm^{-2} (Figure S9). The volumetric energy density and volumetric power density are also shown in the Ragone plot of Figure S10. Our device had achieved the highest volumetric energy density of 1.29 mW h cm^{-3} at a volumetric power density of 53.02 mW cm^{-3}, which is higher than or on par with those of other MnO_x-based asymmetic supercapacitors reported previously (Table 1): CF@rGO@MnO_2//CF@TRGO (1.23 mW h cm^{-3}, 0.27 W cm^{-3}),[50] Mn_3O_4@NGP//Ni(OH)$_2$@NGP (0.35 mW h cm^{-3}, 0.0325 W cm^{-3}),[51] MnO_2@ZnO//HI-rGO (0.234 mW h cm^{-3}, 0.133 W cm^{-3}),[36] rGO//MnO_{2-x} NRs (0.25 mW h cm^{-3}, 1.44 W cm^{-3}),[52] and H-TiO_2@MnO_2//H-TiO_2@C (0.30 mW h cm^{-3}, 0.23 W cm^{-3}).[53] Long-term cycling stability is another critical requirement for supercapacitors. Figure 5d shows the capacitance retention as a function of cycle number at a current density of 2 A g^{-1}. In contrast to many other previously reported transition metal oxide electrodes, our all-solid-state 3D Al@Ni@MnO_x NSP//CCG supercapacitor exhibits excellent cycling stability. It preserved 96.3% of the initial capacitance even after 10000 charge/discharge cycles, which is higher than most MnO_x-based all-solid-state asymmetric supercapacitors: Ni@GF@MnO_2//Ni@GF@PPy (PVA/KOH, 10000 cycles, 90.2%),[54] MnO_x@Au nanocone//CCG (PVA/Na_2SO_4, 2000 cycles, 96.5%),[21] and H-TiO_2@MnO_2// H-TiO_2@C (PVA/LiCl, 5000 cycles, 91.2%).[53]

CONCLUSIONS

In conclusion, we have fabricated all-solid-state asymmetric supercapacitors using a 3D Al@Ni@MnO_x NSP array as the positive electrodes and CCG as the negative electrodes. Compared with the planar MnO_x electrode, the 3D Al@Ni@MnO_x NSP electrode showed remarkable performances with a specific capacitance of 942.2 F g^{-1} and a volumetric capacity of 4.22 F cm^{-3} at a scan rate of 50 mV s^{-1}. The superior performance of the 3D Al@Ni@MnO_x NSP electrode can be attributed to the increase of effective electrode surface area and short electron transfer pathway, as well as facile permeation of electrolyte into the active materirals. The all-solid-state asymmetric supercapacitor could deliver an energy density of 23.02 W h kg^{-1} at current density of 1 A g^{-1} and a volumetric energy capacity of 1.29 mW h cm^{-3} at a volumetric power capacity of 53.02 mW cm^{-3}. The supercapacitor also exhibited good cycling stability with extremely low capacitance loss after 10000 cycles at a current density of 2 A g^{-1}. Overall, this unique 3D NSP array electrode may have the great potential to be used in high-efficiency and low-cost energy-storage devices.

ASSOCIATED CONTENT

Supporting Information

The Supporting Information is available free of charge on the ACS Publications website at DOI: 10.1021/acsami.5b07849.

Other characterizations such as SEM and electrochemical testing data (PDF)

AUTHOR INFORMATION

Corresponding Authors

*(Y.Q.) E-mail: chqiuyc@gmail.com.
*(Y.Z.) E-mail: ygzhang2012@sinano.ac.cn.

Author Contributions

Y.Q. and Y.Z. conceived and designed the experiments. J.Y. assembled the supercapacitor and performed electrochemical tests. G.L. fabricated the NSP structures, and Z.P. performed the MnO_x deposition. Y.H. provided the electrolyte. Y.X. measured XPS spectra. L.S., M.L., X.Z., and H.D. joined in the discussion of the experiment. All authors analyzed data and cowrote the manuscript.

Notes

The authors declare no competing financial interest.

ACKNOWLEDGMENTS

This work was supported by the National Science Foundation for Postdoctoral Scientists of China (014M550314), the Natural Science Foundation of Jiangsu Province, China (BK20140383), New Century Excellent Talents in University (NCET-12-0643), the Natural Science Foundation of Guangdong Province (S4013010012678), and the National Natural Science Foundation of China (Grants 51202137, 21303251, 21171060, 21403287, and 21433013).

REFERENCES

(1) Gao, H.; Xiao, F.; Ching, C. B.; Duan, H. Flexible All-solid-state Asymmetric Supercapacitors Based on Free-standing Carbon Nanotube/Graphene and Mn_3O_4 Nanoparticle/Graphene Paper Electrodes. *ACS Appl. Mater. Interfaces* **2012**, *4*, 7020−7026.

(2) Cheng, Y.; Lu, S.; Zhang, H.; Varanasi, C. V.; Liu, J. Synergistic Effects from Graphene and Carbon Nanotubes Enable Flexible and Robust Electrodes for High-performance Supercapacitors. *Nano Lett.* **2012**, *12*, 4206−4211.

(3) Liu, M.; Tjiu, W. W.; Pan, J.; Zhang, C.; Gao, W.; Liu, T. One-step Synthesis of Graphene Nanoribbon-MnO_2 Hybrids and Their All-solid-state Asymmetric Supercapacitors. *Nanoscale* **2014**, *6*, 4233−4242.

(4) Wang, G.; Wang, H.; Lu, X.; Ling, Y.; Yu, M.; Zhai, T.; Tong, Y.; Li, Y. Solid-State Supercapacitor Based on Activated Carbon Cloths Exhibits Excellent Rate Capability. *Adv. Mater.* **2014**, *26*, 2676−2682.

(5) Chen, P. C.; Shen, G.; Shi, Y.; Chen, H.; Zhou, C. Preparation and Characterization of Flexible Asymmetric Supercapacitors Based on Transition-metal-oxide Nanowire/Single-walled Carbon Nanotube Hybrid Thin-film Electrodes. *ACS Nano* **2010**, *4*, 4403−4011.

(6) Qiu, Y.; Zhao, Y.; Yang, X.; Li, W.; Wei, Z.; Xiao, J.; Leung, S. F.; Lin, Q.; Wu, H.; Zhang, Y.; Fan, Z.; Yang, S. Three-dimensional Metal/oxide Nanocone Arrays for High-performance Electrochemical Pseudocapacitors. *Nanoscale* **2014**, *6*, 3626−3631.

(7) Xu, J.; Wang, Q.; Wang, X.; Xiang, Q.; Liang, B.; Chen, D.; Shen, G. Flexible Asymmetric Supercapacitors Based upon Co_9S_8 Nanorod//Co_3O_4@RuO_2 Nanosheet Arrays on Carbon Cloth. *ACS Nano* **2013**, *7*, 5453−5462.

(8) Xiao, X.; Peng, Z.; Chen, C.; Zhang, C.; Beidaghi, M.; Yang, Z.; Wu, N.; Huang, Y.; Miao, L.; Gogotsi, Y.; Zhou, J. Freestanding MoO_{3-x} Nanobelt/Carbon Nanotube Films for Li-ion Intercalation Pseudocapacitors. *Nano Energy* **2014**, *9*, 355−363.

(9) Lu, X.; Liu, T.; Zhai, T.; Wang, G.; Yu, M.; Xie, S.; Ling, Y.; Liang, C.; Tong, Y.; Li, Y. Improving the Cycling Stability of Metal-Nitride Supercapacitor Electrodes with a Thin Carbon Shell. *Adv. Energy Mater.* **2014**, *4*, 1300994(1)−1300994(6).

(10) Cheng, Y.; Zhang, H.; Lu, S.; Varanasi, C. V.; Liu, J. Flexible Asymmetric Supercapacitors with High Energy and High Power Density in Aqueous Electrolytes. *Nanoscale* **2013**, *5*, 1067−1073.

(11) Zhang, F.; Zhang, T.; Yang, X.; Zhang, L.; Leng, K.; Huang, Y.; Chen, Y. A High-performance Supercapacitor-Battery Hybrid Energy Storage Device Based on Graphene-enhanced Electrode Materials with Ultrahigh Energy Density. *Energy Environ. Sci.* **2013**, *6*, 1623−1632.

DOI: 10.1021/acsami.5b07849
ACS Appl. Mater. Interfaces 2015, 7, 22172−22180

(12) Zhang, J.; Jiang, J.; Li, H.; Zhao, X. S. A High-performance Asymmetric Supercapacitor Fabricated with Graphene-based Electrodes. *Energy Environ. Sci.* **2011**, *4*, 4009−4015.
(13) Zhi, M.; Xiang, C.; Li, J.; Li, M.; Wu, N. Nanostructured Carbon-metal Oxide Composite Electrodes for Supercapacitors: a review. *Nanoscale* **2013**, *5*, 72−88.
(14) Yu, D.; Wang, Y.; Zhang, L.; Low, Z.-X.; Zhang, X.; Chen, F.; Feng, Y.; Wang, H. Three-dimensional Branched Single-crystal Beta-$Co(OH)_2$ Nanowire Array and Its Application for Supercapacitor with Excellent Electrochemical Property. *Nano Energy* **2014**, *10*, 153−162.
(15) Li, J.; Xiao, J.; Wang, Z.; Wei, Z.; Qiu, Y.; Yang, S. Construction of Bicontinuously Porous Ni Architecture as a Deposition Scaffold for High Performance Electrochemical Supercapacitors. *Nano Energy* **2014**, *10*, 329−336.
(16) Yu, M.; Zhai, T.; Lu, X.; Chen, X.; Xie, S.; Li, W.; Liang, C.; Zhao, W.; Zhang, L.; Tong, Y. Manganese Dioxide Nanorod Arrays on Carbon Fabric for Flexible Solid-state Supercapacitors. *J. Power Sources* **2013**, *239*, 64−71.
(17) He, Y. M.; Chen, W. J.; Li, X. D.; Zhang, Z. X.; Fu, J. C.; Zhao, C. H.; Xie, E. Q. Freestanding Three-Dimensional Graphene/MnO_2 Composite Networks as Ultra Light and Flexible Supercapacitor Electrodes. *ACS Nano* **2013**, *7*, 174−182.
(18) Wu, Z. S.; Ren, W.; Wang, D. W.; Li, F.; Liu, B.; Cheng, H. M. High-energy MnO_2 Nanowire/Graphene and Graphene Asymmetric Electrochemical Capacitors. *ACS Nano* **2010**, *4*, 5835−5842.
(19) Wang, Y. S.; Li, S.-M.; Hsiao, S.-T.; Liao, W.-H.; Yang, S.-Y.; Ma, C.C. M.; Hu, C. C. Electrochemical Composite Deposition of Porous Cactus-like Manganese Oxide/Reduced Graphene Oxide-Carbon Nanotube Hybrids for High-Power Asymmetric Supercapacitors. *J. Mater. Chem. C* **2015**, *3*, 4987−4996.
(20) Qiu, K.; Lu, Y.; Zhang, D.; Cheng, J.; Yan, L.; Xu, J.; Liu, X.; Kim, J.-K.; Luo, Y. Mesoporous, Hierarchical Core/Shell Structured $ZnCo_2O_4/MnO_2$ Nanocone Forests for High-Performance Supercapacitors. *Nano Energy* **2015**, *11*, 687−696.
(21) Qiu, Y.; Zhao, Y.; Yang, X.; Li, W.; Wei, Z.; Xiao, J.; Leung, S.-F.; Lin, Q.; Wu, H.; Zhang, Y.; Fan, Z.; Yang, S. Three-Dimensional Metal/Oxide Nanocone Arrays for High-Performance Electrochemical Pseudocapacitors. *Nanoscale* **2014**, *6*, 3626−3631.
(22) Wu, S.; Chen, W.; Yan, L. Fabrication of a 3D MnO_2/Graphene Hydrogel for High-performance Asymmetric Supercapacitors. *J. Mater. Chem. A* **2014**, *2*, 2765−2772.
(23) Fan, Z.; Yan, J.; Wei, T.; Zhi, L.; Ning, G.; Li, T.; Wei, F. Asymmetric Supercapacitors Based on Graphene/MnO_2 and Activated Carbon Nanofiber Electrodes with High Power and Energy Density. *Adv. Funct. Mater.* **2011**, *21*, 2366−2375.
(24) Jin, W. H.; Cao, G. T.; Sun, J. Y. Hybrid supercapacitor based on MnO_2 and Columned FeOOH Using Li_2SO_4 Electrolyte Solution. *J. Power Sources* **2008**, *175*, 686−691.
(25) Grote, F.; Lei, Y. A Complete Three-dimensionally Nanostructured Asymmetric Supercapacitor with High Operating Voltage Window Based on PPy and MnO_2. *Nano Energy* **2014**, *10*, 63−70.
(26) Xiao, X.; Ding, T.; Yuan, L.; Shen, Y.; Zhong, Q.; Zhang, X.; Cao, Y.; Hu, B.; Zhai, T.; Gong, L.; Chen, J.; Tong, Y.; Zhou, J.; Wang, Z. L. WO_{3-x}/MoO_{3-x} Core/Shell Nanowires on Carbon Fabric as an Anode for All-Solid-State Asymmetric Supercapacitors. *Adv. Energy Mater.* **2012**, *2*, 1328−1332.
(27) Ulihin, A. S.; Mateyshina, Y. G.; Uvarov, N. F. All-solid-state Asymmetric Supercapacitors with Solid Composite Electrolytes. *Solid State Ionics* **2013**, *251*, 62−65.
(28) Gao, H.; Lian, K. High Rate All-Solid Electrochemical Capacitors Using Proton Conducting Polymer Electrolytes. *J. Power Sources* **2011**, *196*, 8855−8857.
(29) Lian, K.; Tian, Q. Solid Asymmetric Electrochemical Capacitors Using Proton-Conducting Polymer Electrolytes. *Electrochem. Commun.* **2010**, *12*, 517−519.
(30) Yang, X.; Cheng, C.; Wang, Y.; Qiu, L.; Li, D. Liquid-Mediated Dense Integration of Graphene Materials for Compact Capacitive Energy Storage. *Science* **2013**, *341*, 534−537.
(31) Khomenko, V.; Raymundo-Piñero, E.; Frackowiak, E.; Béguin, F. High-Voltage Asymmetric Supercapacitors Operating in Aqueous Electrolyte. *Appl. Phys. A: Mater. Sci. Process.* **2006**, *82*, 567−573.
(32) Qu, Q. T.; Shi, Y.; Tian, S.; Chen, Y. H.; Wu, Y. P.; Holze, R. A New Cheap Asymmetric Aqueous Supercapacitor: Activated Carbon//$NaMnO_2$. *J. Power Sources* **2009**, *194*, 1222−1225.
(33) Hu, L.; Chen, W.; Xie, X.; Liu, N.; Yang, Y.; Wu, H.; Yao, Y.; Pasta, M.; Alshareef, H. N.; Cui, Y. Symmetrical MnO_2-Carbon Nanotube-Textile Nanostructures for Wearable Pseudocapacitors with High Mass Loading. *ACS Nano* **2011**, *5*, 8904−8913.
(34) Cottineau, T.; Toupin, M.; Delahaye, T.; Brousse, T.; Belanger, D. Nanostructured Transition Metal Oxides for Aqueous Hybrid Electrochemical Supercapacitors. *Appl. Phys. A: Mater. Sci. Process.* **2006**, *82*, 599−606.
(35) Jessensky, O.; Muller, F.; Gosele, U. Self-Organized Formation of Hexagonal Pore Arrays in Anodic Alumina. *Appl. Phys. Lett.* **1998**, *72*, 1173−1175.
(36) Wang, Z.; Zhu, Z.; Qiu, J.; Yang, S. High Performance Flexible Solid-State Asymmetric Supercapacitors from MnO_2/ZnO Core−Shell Nanorods//Specially Reduced Graphene Oxide. *J. Mater. Chem. C* **2014**, *2*, 1331−1336.
(37) Sumboja, A.; Foo, C. Y.; Wang, X.; Lee, P. S. Large Areal Mass, Flexible and Free-Standing Reduced Graphene Oxide/Manganese Dioxide Paper for Asymmetric Supercapacitor Device. *Adv. Mater.* **2013**, *25*, 2809−2815.
(38) Nam, K. W.; Kim, K. B. Manganese Oxide Film Electrodes Prepared by Electrostatic Spray Deposition for Electrochemical Capacitors. *J. Electrochem. Soc.* **2006**, *153*, A81−A88.
(39) Buciuman, F.; Patcas, F.; Craciun, R.; Zahn, D. R. T. Vibrational Spectroscopy of Bulk and Supported Manganese Oxides. *Phys. Chem. Chem. Phys.* **1999**, *1*, 185−190.
(40) Xiao, F.; Xu, Y. Pulse Electrodeposition of Manganese Oxide for High-Rate Capability Supercapacitors. *Int. J. Electrochem. Sci.* **2012**, *7*, 7440−7450.
(41) Song, M. K.; Cheng, S.; Chen, H.; Qin, W.; Nam, K. W.; Xu, S.; Yang, X. Q.; Bongiorno, A.; Lee, J.; Bai, J.; Tyson, T. A.; Cho, J.; Liu, M. Anomalous Pseudocapacitive Behavior of A Nanostructured, Mixed-Valent Manganese Oxide Film for Electrical Energy Storage. *Nano Lett.* **2012**, *12*, 3483−3490.
(42) Conway, B. E. *Electrochemical Supercapacitors: Scientific Fundamentals and Technological Applications*; Kluwer Academic Publishers, Plenum Press: New York, 1999.
(43) Gao, H.; Xiao, F.; Ching, C. B.; Duan, H. High-Performance Asymmetric Supercapacitor Based on Graphene Hydrogel and Nanostructured MnO_2. *ACS Appl. Mater. Interfaces* **2012**, *4*, 2801−2810.
(44) Shao, Y.; Wang, H.; Zhang, Q.; Li, Y. High-Performance Flexible Asymmetric Supercapacitors Based on 3D Porous Graphene/MnO_2 Nanorod and Graphene/Ag Hybrid Thin-Film Electrodes. *J. Mater. Chem. C* **2013**, *1*, 1245−1251.
(45) Lei, Z.; Zhang, J.; Zhao, X. S. Ultrathin MnO_2 Nanofibers Grown on Graphitic Carbon Spheres as High-Performance Asymmetric Supercapacitor Electrodes. *J. Mater. Chem.* **2012**, *22*, 153−160.
(46) Liu, Y.; He, D.; Wu, H.; Duan, J.; Zhang, Y. Hydrothermal Self-Assembly of Manganese Dioxide/Manganese Carbonate/Reduced Graphene Oxide Aerogel for Asymmetric Supercapacitors. *Electrochim. Acta* **2015**, *164*, 154−162.
(47) Wang, G.; Xu, H.; Lu, L.; Zhao, H. One-Step Synthesis of Mesoporous MnO_2/Carbon Sphere Composites for Asymmetric Electrochemical Capacitors. *J. Mater. Chem. A* **2015**, *3*, 1127−1132.
(48) Deng, L.; Zhu, G.; Wang, J.; Kang, L.; Liu, Z.-H.; Yang, Z.; Wang, Z. Graphene-MnO_2 and Graphene Asymmetrical Electrochemical Capacitor with a High Energy Density in Aqueous Electrolyte. *J. Power Sources* **2011**, *196*, 10782−10787.
(49) Khomenko, V.; Raymundo-Piñero, E.; Béguin, F. Optimisation of an Asymmetric Manganese Oxide/Activated Carbon Capacitor Working at 2V in Aqueous Medium. *J. Power Sources* **2006**, *153*, 183−190.

DOI: 10.1021/acsami.5b07849
ACS Appl. Mater. Interfaces 2015, 7, 22172−22180

(50) Zhang, Z.; Xiao, F.; Xiao, J.; Wang, S. Functionalized Carbonaceous Fibers for High Performance Flexible All-Solid-State Asymmetric Supercapacitors. *J. Mater. Chem. A* **2015**, *3*, 11817−11823.
(51) Feng, J. X.; Ye, S. H.; Lu, X. F.; Tong, Y. X.; Li, G. R. Asymmetric Paper Supercapacitor Based on Amorphous Porous Mn_3O_4 Negative Electrode and $Ni(OH)_2$ Positive Electrode: A Novel and High-Performance Flexible Electrochemical Energy Storage Device. *ACS Appl. Mater. Interfaces* **2015**, *7*, 11444−11451.
(52) Zhai, T.; Xie, S.; Yu, M.; Fang, P.; Liang, C.; Lu, X.; Tong, Y. Oxygen Vacancies Enhancing Capacitive Properties of MnO_2 Nanorods for Wearable Asymmetric Supercapacitors. *Nano Energy* **2014**, *8*, 255−263.
(53) Lu, X.; Yu, M.; Wang, G.; Zhai, T.; Xie, S.; Ling, Y.; Tong, Y.; Li, Y. H-TiO_2@MnO_2//H-TiO_2 @C Core-Shell Nanowires for High Performance and Flexible Asymmetric Supercapacitors. *Adv. Mater.* **2013**, *25*, 267−272.
(54) Zhang, Z.; Chi, K.; Xiao, F.; Wang, S. Advanced Solid-State Asymmetric Supercapacitors Based on 3D Graphene/MnO_2 and Graphene/Polypyrrole Hybrid Architectures. *J. Mater. Chem. A* **2015**, *3*, 12828−12835.

DOI: 10.1021/acsami.5b07849
ACS Appl. Mater. Interfaces 2015, 7, 22172−22180